Differential cross section and analyzing power of the $\vec{p}\,p \rightarrow pp\pi^0$ reaction at a beam energy of 390 MeV

Y. Maeda,[1,2,*] M. Segawa,[1,†] T. Ishida,[3,‡] A. Kacharava,[2,4] M. Nomachi,[5] Y. Shimbara,[5,§] Y. Sugaya,[5] K. Tamura,[6] T. Yagita,[3] K. Yasuda,[7] H. P. Yoshida,[1,‖] and C. Wilkin[8]

[1]*Research Center for Nuclear Physics, Osaka University, Ibaraki, Osaka 567-0047, Japan*
[2]*Institut für Kernphysik, Forschungszentrum Jülich, D-52425 Jülich, Germany*
[3]*Department of Physics, Kyushu University, Fukuoka 812-8581, Japan*
[4]*High Energy Physics Institute, Tbilisi State University, 0186 Tbilisi, Georgia*
[5]*Department of Physics, Osaka University, Toyonaka, Osaka 560-0043, Japan*
[6]*Physics Division, Fukui Medical University, Fukui 910-1193, Japan*
[7]*The Wakasa Wan Energy Research Center, Fukui 914-0192, Japan*
[8]*Physics and Astronomy Department, UCL, Gower Street, London WC1E 6BT, United Kingdom*

(Received 16 February 2008; published 16 April 2008)

The differential cross section and analyzing power A_y of the $\vec{p}\,p \rightarrow pp\pi^0$ reaction have been measured at RCNP in coplanar geometry at a beam energy of 390 MeV and the dependence on both the pion emission angle and the relative momentum of the final protons has been extracted. The angular variation of A_y for the large values of the relative momentum studied here shows that this is primarily an effect of the interference of pion s and p waves and this interference can also explain the momentum dependence. Within the framework of a very simple model, these results would suggest that the pion-production operator has a significant long-range component.

DOI: 10.1103/PhysRevC.77.044004 PACS number(s): 24.70.+s, 13.75.Cs, 13.60.Le, 25.40.Ve

I. INTRODUCTION

Pion production is the first and probably the simplest of the inelastic processes in nucleon-nucleon collisions and its understanding may provide us with valuable information about low- and medium-energy strong interaction physics. Motivated by this, over the past decade there has been a series of detailed studies of the $pp \rightarrow pp\pi^0$ reaction from near the production threshold up to a proton beam energy of 425 MeV. These have been carried out at several laboratories: IUCF [1,2], TSL [3–5], and COSY-TOF [6,7].

Initial theoretical calculations [8] for π^0 production estimated a total cross section that was one-fifth that of experiment [1]. This indicated clearly that some essential mechanism was missing from the theory of s-wave pion production leading to the S state of the final protons. Lee and Riska [9] suggested that this might be connected with short-range effects between nucleons, and quantitative support for this was found in a model with the exchange of a heavy meson coupled to the antinucleon-nucleon pair [10]. However, it has been claimed that s-wave pion rescattering is not small [11,12] and that one can reproduce the cross section data without invoking short-range effects [11]. Studies based on chiral perturbation theory (χPT) [13–16] show that the contribution of pion rescattering is indeed sizable but that the sign of this term is opposite to that of Refs. [11,12], and this leads to an even more severe discrepancy between theory and experiment. The convergence of the chiral expansion can be seriously questioned for s-wave pion production because of the large momentum transfer between nucleons, whereas the expansion seems to show convergence in the case of the p-wave pion [17]. An ordering scheme has since been discussed [18]. Thus the origin of s-wave pion production remains unclear even as to whether or not the production mechanism is dominated by short-range effects.

Differential cross sections and polarization observables have been measured at several bombarding energies [2,4,5,7] and theoretical estimates of these observable have been made by groups at Jülich [19] and Osaka [20]. Both approaches include higher partial waves and provide good fits to the total cross section close to threshold. However, the differential and polarization observables are not well reproduced by either group. To try to identify the origin of the problem more clearly it may be useful to attempt a partial-wave decomposition. In Ref. [2], the angular dependencies of the different polarization observables were developed by using a general formalism consisting of a complete set of functions, with coefficients extracted by fitting data, and this has been extended in later work [21]. However, because of the limited accuracy of polarization data existing at the time, the analysis was done by assuming that only a small number of partial waves contributed and that the momentum dependence of these amplitude stemmed purely from the centrifugal barrier. This

*ymaeda@rcnp.osaka-u.ac.jp
†Present address: Nuclear Science Research Institute, Tokai Research and Development Center, Tokai-mura, Naka-gun, Ibaraki 319-1195, Japan.
‡Present address: Laboratory of Nuclear Science, Tohoku University, Sendai, Miyagi 982-0826, Japan.
§Present address: National Superconducting Cyclotron Laboratory, Michigan State University, East Lansing, Michigan 48824-1321, USA.
‖Present address: Cyclotron and Radioisotope Center, Tohoku University, Sendai, Miyagi 980-8578, Japan.

latter assumption is very doubtful since, for the P state of final protons, it does not lead to a good description of the differential cross section [4]. More precise data on the angular and momentum dependence of the polarization observables, as well as of the differential cross section, are highly desirable. The accumulation of such data may allow one to perform a fuller partial-wave analysis of the $pp \to pp\pi^0$ reaction, which would provide greater insight for the theoretical models.

We report here a measurement of the $\vec{p}p \to pp\pi^0$ reaction at a beam energy of 390 MeV, where the beam polarization is perpendicular to the plane containing the detectors. The differential cross section and analyzing power A_y are obtained as functions of the pion emission angle θ_q in the center-of-mass system and the relative momentum p of the final protons. The use of a high-intensity polarized beam in conjunction with a liquid hydrogen target makes it possible to extract the angular dependence of A_y for different ranges in p. Such data, which have not been available previously, might offer serious constraints on theoretical models.

If only a few partial waves are important, the angular dependence of the $A_y \times$ spin-averaged cross section is composed of terms proportional to $\sin\theta_q$ and $\sin 2\theta_q$. The strength of the $\sin\theta_q$ term is governed by the interference of amplitudes corresponding to the production of Ps and Pp final states. Here, in standard notation, the final states are labeled by Ll, where L and l are the angular momenta of the proton pair and the pion, respectively. The $\sin 2\theta_q$ strength is determined by S and higher states.

The variation with the momentum p, obtained after integration over angles, is sensitive to the Ps and Pp production amplitudes. This is studied in a model where it is assumed that the momentum dependence of the proton-proton wave functions in the final state is the main influence for the P-state amplitudes. Furthermore, in a very simplistic approach, the wave functions are evaluated at a *fixed* proton-proton separation distance.

The experimental facility, and in particular the detectors, polarized beam, and target, are described in Sec. II. Section III is devoted to the steps needed to identify and measure the $pp \to pp\pi^0$ reaction. The extraction of the observables from data taken under our specific kinematic conditions, where the detection system is essentially coplanar, is the subject of Sec. IV, with the experimental results being shown in Sec. V. The general features of the angular and momentum dependence of the cross section and analyzing powers are given in Sec. VI. It is shown there that, when comparing our results with published data that have large acceptance, it is crucial to take account of our particular coplanar geometry. Section VII presents the simple phenomenological description of pion production. Our conclusions are given in Sec. VIII.

II. EXPERIMENT

The experiment was carried out by using a 390-MeV polarized proton beam extracted from the cyclotron complex at the Research Center for Nuclear Physics (RCNP), Osaka. The polarized beam was produced by an atomic-beam-type polarized ion source with an electron cyclotron resonance (ECR) ionizer [22], where the polarization state ("up" or "down") of the primary beam was reversed with a frequency of 1 Hz. The protons were first accelerated in the injector AVF cyclotron before being further accelerated to 390 MeV in the main cyclotron ring. After extraction, the vertically polarized beam was transported to the scattering chamber in the experimental hall. Figure 1 shows the top view of the scattering chamber as well as of our detection system. The scattering chamber containing a liquid hydrogen target consisted of an evacuated vertical cylinder. The window made of an aramid foil had a horizontal opening angle from 15° to 110° on either side of the the beam direction. After hitting the target the primary beam was transported to the beam dump where a Faraday cup monitored the beam intensity for the two polarization states. The beam current was limited to around 1 nA to minimize the dead time of the data acquisition system. Under these conditions the system, the details of which are described in Ref. [23], had an efficiency of between 75% and 87%.

A. Detector

The detector system was symmetric with respect to the plane containing the beam axis and the direction of the beam

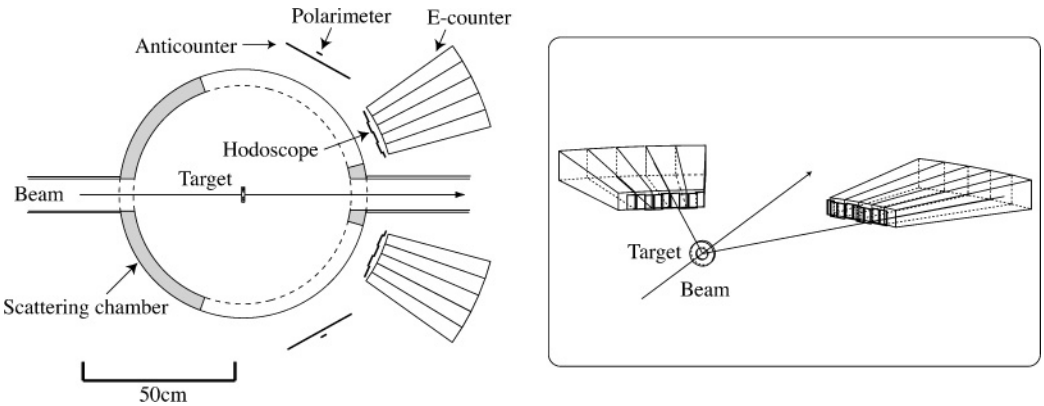

FIG. 1. Top view of the layout of the experiment. The shaded region shows the walls of the target chamber and the dashed lines its windows. In the right-hand panel a three-dimensional sketch shows the positions of the hodoscope and E-counters.

polarization. The two outgoing protons from the $pp \to pp\pi^0$ reaction were detected simultaneously in an array of plastic scintillators. The measurement of two pairs of polar and azimuthal angles and two kinetic energies is sufficient to identify the $pp \to pp\pi^0$ reaction and determine the five independent kinematic variables. The system covered laboratory polar angles $15^\circ < \theta < 35^\circ$. The maximum angle of protons from the $pp \to pp\pi^0$ reaction at 390 MeV (32.1°) is well inside the angular acceptance. The minimum angle was limited for both protons such that only proton pairs with relative momenta from 150 MeV/c up to the kinematic limit of 220 MeV/c could be registered with this system. The detector was therefore well suited for the investigation of the high relative momentum region, where the pion-production amplitudes leading to P-state proton pairs should have their maximum strength. However, it is important to note that the c.m. polar angle of the relative momentum vector for final protons was confined to $90^\circ \pm 30^\circ$ with respect to the beam axis.

The energy of a scattered proton was deduced from the amplitude signal in one of the E-counters. Such a counter consists of a set of five plastic scintillators in which each element has a trapezoidal shape, with front and back faces of area 35×35 mm^2 and 60×60 mm^2, respectively. The 350-mm length is sufficient to stop protons with energies up to 250 MeV so that all protons from the $pp \to pp\pi^0$ reaction at 390 MeV were stopped. The front face of each counter was positioned 500 mm from the target. The scintillator hodoscopes in front of the counters were used to determine the directions of outgoing particles; a single 3-mm-thick element of area 17.5×30 cm^2 covered ± 17 mrad horizontally and ± 30 mrad vertically. Two elements were placed in front of each of four E-counters with a 1-mm overlap, though only one element was used for the counter at the largest angle. There was thus a total of nine elements on each side of the beam. The angle of the detected particle was defined by the center of each element.

The anticoincidence counter (marked "Anticounter" in Fig. 1) was used to eliminate accidental events coming from elastic proton-proton scattering. This covered the angular range 45°–72°, where recoil protons from the elastic scattering hit the counter in combination with the scintillator hodoscopes. The information from the counter was used in the offline analysis and about 90% of the accidentals could be suppressed in this way.

One hodoscope element and a scintillation counter placed at $60^\circ \pm 1^\circ$ (denoted as the "Polarimeter" in Fig. 1) were used to monitor the beam polarization. The fast and recoil protons from elastic proton-proton scattering were detected in coincidence. According to the SAID database [24], the $pp \to pp$ analyzing power at this energy and angle is $A_y = -0.364 \pm 0.007$, where the error bar has been obtained by looking at typical data in this region. The average values of the beam polarizations deduced on this basis were $P_\uparrow = 0.66 \pm 0.01$ and $P_\downarrow = 0.70 \pm 0.01$, where the arrows indicate the spin states of the proton beam and the errors are statistical. The polarizations were quite stable during the experiment and all values lay within about ± 0.03 of the averages.

B. Target

The liquid hydrogen (LH_2) target was 8.5 mm thick, with windows made of 25-μm-thick aramid foil [25]. Its temperature was controlled in the range of 14 to 20 K and kept stable at 17.6 ± 0.4 K during experimental runs. The *empty target* runs, which were carried out with hydrogen gas at temperatures between 22 and 27 K, were used to estimate the background from other construction materials as well as from the residual gas frozen on the windows.

C. Data taking

A signal was registered when a charged particle hit both of the scintillator hodoscopes and the corresponding E-counter. For the measurement of the $pp \to pp\pi^0$ reaction, the trigger conditions were set so that both right- and left-side counters were required to give signals in coincidence. In addition, measurements without the coincidence requirement were also performed to detect single protons from elastic proton-proton scattering. Such measurements were also performed by using an unpolarized proton beam to check the determination of the luminosity as well as of the beam polarization. These are the subject of the following section.

III. DATA ANALYSIS

A. Particle identification

Particle identification was achieved by the ΔE-E method. The amplitude signal, related to the energy loss in the scintillator hodoscope, is plotted in Fig. 2 against the amplitude signal from the E-counter. The heavily populated band arises from protons, associated mostly with π^0 production, that stopped inside the counter. The $pp \to pp\pi^0$ events of interest are well separated from the two lower islands. These are

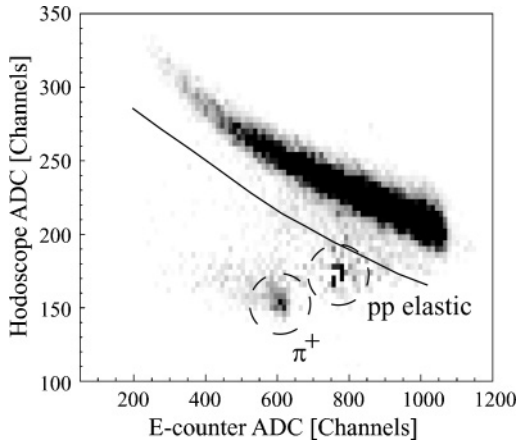

FIG. 2. Identification of protons from the $pp \to pp\pi^0$ reaction. The signal from the hodoscope is plotted versus that from the E-counter. The intense band is due to protons that have stopped in the scintillator. Groups of events corresponding to elastically scattered protons and pions from the $pp \to pn\pi^+$ reaction are indicated and separated by the cut shown as the solid line.

produced by elastically scattered protons, which have energies above 265 MeV and thus do not stop inside the counter, and positive pions generated through the $pp \rightarrow pn\pi^+$ reaction.

B. Energy calibration of the *E*-counter

At a beam energy of 390 MeV, the energies of the detected protons from the $pp \rightarrow pp\pi^0$ reaction varied between 40 and 226 MeV. The energy dependence of the amplitude signal from the E-counter could be calibrated above 100 MeV by using elastic proton-proton scattering events. The hodoscope and E-counter were set to cover the angular range 40°–60° and, for an angle fixed by the hodoscope, the monoenergetic recoil proton was measured by an E-counter element. The energy resolution was found to be better than 2% (FWHM) for a proton energy of 200 MeV.

Below 100 MeV, information from the $pp \rightarrow pp\pi^0$ reaction itself was used. Figures 3(a) and 3(b) show, respectively, the simulated and measured energy correlation between protons that hit a pair of hodoscope elements to the right and left of the beam. The locus of π^0 events can be clearly seen and this was used to extract a data sample where the energy in the left (right) counter was higher than 100 MeV, while that in the right (left) was lower, as indicated by Case 1(2) in Fig. 3(a). In addition a pedestal value from the analog-to-digital converter (ADC) module was also used at an energy of 17 MeV,

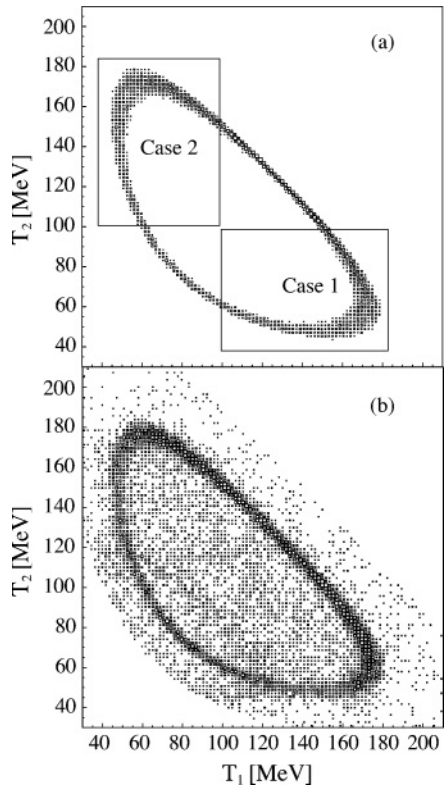

FIG. 3. Two-dimensional plot of the proton energy T_2 deposited in the right-hand E-counter versus the same quantity T_1 for the left-hand counter. The hodoscope elements, located closest to the beam line on both sides, were selected. Panels (a) and (b) show the simulated and experimental data, respectively.

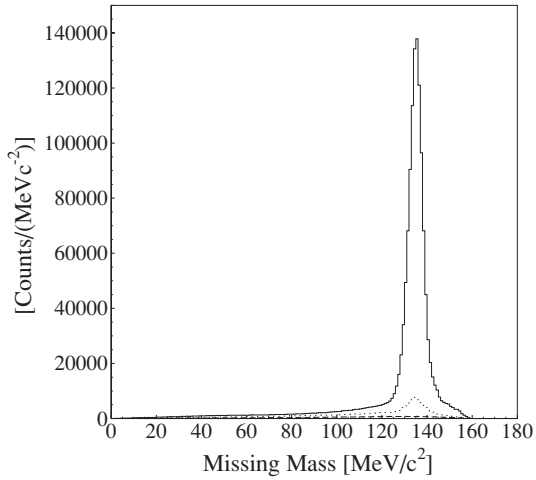

FIG. 4. The $pp \rightarrow ppX^0$ missing-mass spectrum obtained for all geometric configurations using the LH_2 (solid histogram) and the gaseous hydrogen target of the "empty run" (dotted line). The estimate of random coincidence events is shown by the dashed line. The peak corresponding to π^0 production has a mass of 135.0 MeV/c^2 and a width of 7.4 MeV/c^2 (FWHM).

corresponding to the minimum energy of protons detected in the E-counter. In this way, the amplitude signals for all combinations of right- and left-side counters were calibrated using third-order polynomials with an accuracy of better than 4%, as judged from the position and width of the resulting π^0 missing-mass peak.

C. Identification of the $pp \rightarrow pp\pi^0$ reaction

Having measured the energies and angles of the two protons, we selected good events on the basis of the missing-mass spectrum. A clear π^0 peak, with a width of 7.4 MeV/c^2 (FWHM), is seen in Fig. 4, which shows the totality of events obtained with the LH_2 target. The background from the target foil was subtracted by utilizing the *empty target* runs normalized to the integrated beam intensity. The contribution from the random coincidences was estimated by considering outgoing protons from different beam bunches. The correspondence of the peak position with the mass of the π^0 is consistent with the energy calibration of the counters.

For all $pp \rightarrow pp\pi^0$ candidates, the pion emission angle θ_q and the relative momentum p and its angle θ_p in the overall center-of-mass system were reconstructed on an event-by-event basis. The data were then grouped in nine intervals in θ_q and three in p, with a finer binning in p being used to study the momentum dependence of the analyzing power.

Missing-mass spectra were constructed for each combination of bins and spin states and used to extract the yield of π^0 events. The backgrounds from random coincidences and target foils were subtracted before compiling the data shown in Fig. 5 for typical conditions. There is some residual background for $\theta_q < 20°$, whose shape varies with the kinematic conditions. This arises from "nonfull" events where, in contrast to "full" events, recoil protons from π^0 production do not

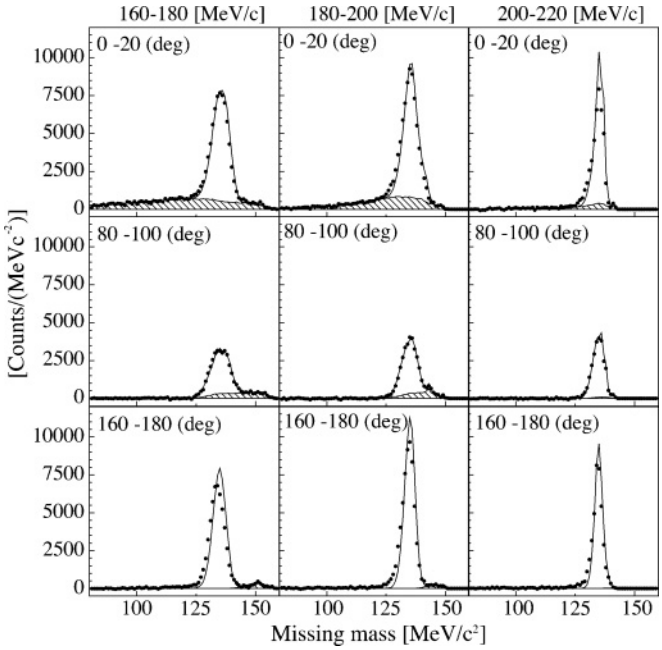

FIG. 5. The $pp \rightarrow ppX^0$ missing-mass spectra for different selected kinematic regions, with the relative momentum p being indicated at the top of the panels and the angle of the pion θ_q being shown within each. The experimental data are presented after subtracting the backgrounds from the random coincidences and target window. The hatched regions show normalized distributions of "nonfull" events, where not all of the energy is deposited in the scintillator. The solid lines show the sums of these plus the good events. The shapes of both distributions have been determined through simulations with GEANT3 [26].

deposit their full energy in the E-counter owing to a nuclear reaction in the scintillator material.

The shapes of the distributions for nonfull and full events were simulated in a Monte Carlo program based on GEANT3 [26], which took into account the energy resolution of the scintillator material, as well as hadronic and electromagnetic interactions. The simulated events were passed through the same analysis chain as the measured data and fitted to the results shown in Fig. 5. The normalization of the nonfull events was determined from the tails of the distributions. To check the systematic uncertainty in the treatment of the nonfull background, the π^0 yield was also determined by selecting all events around the pion peak without any subtraction, and the corresponding uncertainty is discussed in Sec. V.

D. Detection efficiency of E-counters for full events

The detection efficiency for full events, where protons deposit their full energy inside an E-counter, was estimated by using the data obtained for the energy calibration of the E-counters discussed in Sec. III B. The efficiency varies between 0.85 and 0.65 over the measured energy range of 100 to 200 MeV. The efficiency obtained by the Monte Carlo simulation was checked by comparing it with that obtained from the measurement. The two results are in agreement to within 15% and this is included in the overall uncertainty quoted for the cross section.

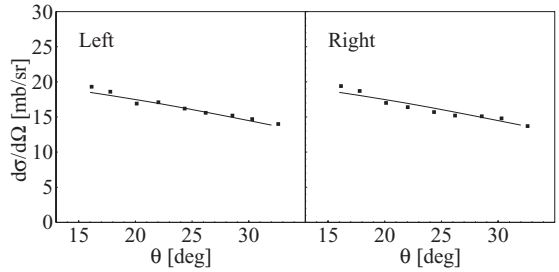

FIG. 6. The laboratory differential cross sections measured for elastic proton-proton scattering using hodoscopes placed to the left and right of the beam. The lines are predictions taken from the SAID database [24].

E. Luminosity

The absolute value of the luminosity was determined from measurements of the beam intensity and the density of the LH_2 target and this gave an integrated luminosity of 16.1 pb^{-1}. The value was verified by measuring elastic proton-proton scattering by identifying single protons through the ΔE-E method. The unpolarized $pp \rightarrow pp$ differential cross sections obtained in this way are shown separately in Fig. 6 for the same angular interval to the left and right of the beam direction. The results agree on average to within $\pm 2\%$ with the predictions of the SAID program [24]. However, there are fluctuations of up to $\pm 5\%$ around the predicted curves and these deviations were included in the determination of the acceptance as corrections associated with the geometrical uncertainties of individual hodoscope elements.

F. Beam polarization

The beam polarizations were also checked by measuring elastic proton-proton scattering where the selection criteria for a single proton is the same as that discussed previously. The analyzing powers obtained in the offline analysis on the basis of the already determined beam polarizations $P_{\uparrow,\downarrow}$ are shown in Fig. 7 for the same laboratory angular range to

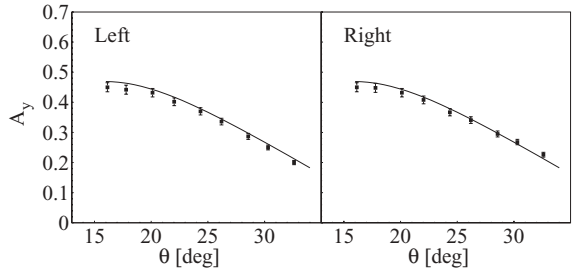

FIG. 7. The analyzing power for elastic proton-proton scattering measured by detecting single protons with hodoscopes placed to the left and right of the beam, using beam polarizations determined by the coincidence method. The lines are estimates taken from the SAID database [24].

the left and right of the beam direction. The results are consistent with those given by the SAID program [24] and the systematic uncertainty in the determination of the beam polarizations, including that coming from the SAID database, was found to be below 6%.

IV. OBSERVABLES

A. Definition

Five independent variables ξ are required to describe the three-body final state and these we take from the relative momentum **p** of the two final protons and that of the pion **q** in the overall c.m. system. Since the magnitudes of these momenta are linked by energy conservation, the resulting set of variables consists of the magnitude of **p** plus two polar angles θ with respect to the beam axis and two azimuthal angles ϕ (i.e., $\xi \equiv \{\theta_q, \varphi_q, \theta_p, \varphi_p, p\}$). The corresponding differential cross section will be denoted

$$\sigma(\xi, P_y) \equiv \frac{d\sigma}{d\Omega_q d\Omega_p dp}. \tag{1}$$

In terms of the Cartesian observables, the dependence of the cross section on the vertical polarization P_y is given by

$$\sigma(\xi, P_y) = \sigma_0(\xi)[1 + P_y A_y(\xi)], \tag{2}$$

where σ_0 is the spin-averaged cross section.

Our goal is to obtain the spin-averaged cross section and analyzing power at the polar angle of $\theta_p = 90^\circ$ in coplanar geometry (i.e., $\varphi_p = \varphi_q = 0^\circ$). These observables are obtained from the experimental data through

$$\sigma_0 = \frac{(P_\downarrow L_\downarrow N_\uparrow + P_\uparrow L_\uparrow N_\downarrow)}{\epsilon L_\uparrow L_\downarrow (P_\downarrow + P_\uparrow)}, \tag{3}$$

$$A_y = \frac{(L_\downarrow N_\uparrow - L_\uparrow N_\downarrow)/\langle \cos\varphi_q \rangle}{(P_\downarrow L_\downarrow N_\uparrow + P_\uparrow L_\uparrow N_\downarrow)}, \tag{4}$$

where $N_{\uparrow,\downarrow}$ is the spin-dependent yield, $P_{\uparrow,\downarrow}$ is the beam polarization, and $L_{\uparrow,\downarrow}$ is the luminosity. The detection efficiency ϵ includes that of the data acquisition system and the acceptance of the detector system, as determined by the Monte Carlo simulation using the phase-space model. The average value of the cosine of the pion angle, $\langle \cos\varphi_q \rangle$, is also determined through the Monte Carlo simulation, as discussed in Sec. V.

B. Angular dependence

For the following discussion it is convenient here to describe the angular dependence expected for the unpolarized cross section and analyzing power of the $pp \to pp\pi^0$ reaction. These, as well as other observables, have been discussed in terms of partial-wave amplitudes in Ref. [2], where total orbital angular momentum excitations up to $L_{pp} + \ell_\pi = 2$ were considered. By taking $\varphi_p = 0^\circ$ and $\theta_p = 90^\circ$, the relevant formulas reduce to

$$\begin{aligned}\sigma_0(\theta_q, \varphi_q, p) &= E + F_1 + H_0^{00} - \left(H_2^{00} + F_2 + K\right) + \left(I + H_1^{00} - H_3^{00}\right) \\ &\quad \times (3\cos^2\theta_q - 1) + H_5^{00} \sin^2\theta_q \cos 2\varphi_q,\end{aligned} \tag{5}$$

$$\begin{aligned}\sigma_0 A_y(\theta_q, \varphi_q, p) &= \left\{\left(G_1^{y0} - G_2^{y0} + G_4^{y0}\right)\sin\theta_q \right. \\ &\quad \left. + \left(I^{y0} + H_1^{y0} - H_2^{y0} + H_5^{y0}\right)\sin 2\theta_q\right\}\cos\varphi_q,\end{aligned} \tag{6}$$

where each of the coefficients is a function of the relative momentum p. The coefficients E, F, and H represent the absolute squares of amplitudes leading to Ss, Ps, and Pp states, respectively, whereas those with G, I, and K reflect the interferences of type $PsPp$, $SsSd$, and $SsDs$, respectively [2].

V. RESULTS

The measured values of the spin-averaged cross section and the analyzing power are shown in Table I as functions of the pion polar angle θ_q for three ranges in the relative momentum p. The mean values and uncertainties in the determination of θ_q have been estimated from the Monte Carlo simulations, where possible fluctuations in the beam energy and geometrical uncertainties in the detector system were taken into account.

The combinations of up-down beam polarizations and left-right detectors provide two measurements of A_y as well as of the spin-averaged cross section, and these should be consistent. However, because of the uncertainty of the energy calibration of the E-counters on the two sides, the data show systematic differences between these combinations. The deviations from the mean value were included in the systematic error for an individual angular bin. Compared with this, the uncertainty resulting from the treatment of the nonfull events as discussed in Sec. III C is negligible for A_y, though it is the dominant systematic error for the spin-averaged cross section.

The size of the θ_p angular bin is quite large ($90^\circ \pm 30^\circ$) and so the analysis was repeated by using the smaller angular interval ($90^\circ \pm 10^\circ$) to estimate the resulting uncertainty. The results for the spin-averaged cross section agree to within 5%, whereas the analyzing power results are in agreement to within the statistical errors. The overall systematic uncertainty for the spin-averaged cross section was estimated to be less than 16% when the uncertainties from the efficiency of full events and the angular bin were taken into account. As mentioned in Sec. III F, the overall systematic uncertainty in A_y coming from the determination of the beam polarization is believed to be less than 6%.

It is important to note that, because of the finite size of our counters, the data were not taken strictly at azimuthal angles $\varphi_q = 0^\circ(180^\circ)$ and the effects of this angular spread increase when θ_q approaches $0^\circ(180^\circ)$ and p gets close to its maximum allowed value. In Table I we show estimates of the average values of $\langle \cos\varphi_q \rangle$ and $\langle \cos 2\varphi_q \rangle$ evaluated using our simulation. It is seen from Eq. (6) that the product $\sigma_0 A_y$ is proportional to $\cos\varphi_q$ but is independent of $\cos 2\varphi_q$ and so the estimates of $\langle \cos\varphi_q \rangle$ have been used in Eq. (4) to deduce A_y. There is an explicit $\cos 2\varphi_q$ in Eq. (5), which means that the value of σ_0 that we have measured is different from that at $\varphi_q = 0^\circ$. As a consequence, when dividing $\sigma_0 A_y$ by σ_0 to derive the analyzing power A_y, some φ_q dependence still remains.

TABLE I. The spin-averaged $pp \to pp\pi^0$ cross section σ_0 and analyzing power A_y measured in different ranges of relative momentum p at the polar angle of $\theta_p = 90^\circ$ with its angular bin of $\pm 30^\circ$. The first and second error bars in σ_0 and A_y show, respectively, the statistical and systematic uncertainties, whereas that for the pion emission angle θ_q is the standard deviation that includes the effects of the binning. The overall systematic uncertainty for A_y is estimated to be less than 6% and that for σ_0 to be less than 16% and these are not included in the systematic uncertainties for an individual angular bin. The observables have been obtained at the average values of $\langle \cos 2\varphi_q \rangle$, whereas the value of $\langle \cos \varphi_q \rangle$ is involved in the evaluation of A_y. To get estimates of the values at $\cos 2\varphi_q = 1$, the cross section should be divided by the correction factor d_t and the analyzing power multiplied by the same factor, as discussed in the text.

θ_q (deg)	p (MeV/c)	σ_0 [nb /(sr^2 MeV c^{-1})]	A_y	$\langle \cos \varphi_q \rangle$	$\langle \cos 2\varphi_q \rangle$	d_t
14 ± 7		$7.64 \pm 0.03 \pm 0.16$	$-0.085 \pm 0.008 \pm 0.005$	0.653	0.206	1.01
31 ± 7		$7.26 \pm 0.03 \pm 0.19$	$-0.191 \pm 0.006 \pm 0.018$	0.950	0.810	1.01
50 ± 7		$5.84 \pm 0.02 \pm 0.23$	$-0.259 \pm 0.007 \pm 0.005$	0.977	0.910	1.02
70 ± 7		$4.89 \pm 0.03 \pm 0.38$	$-0.345 \pm 0.009 \pm 0.047$	0.984	0.938	1.02
90 ± 7	160–180	$4.92 \pm 0.03 \pm 0.23$	$-0.362 \pm 0.018 \pm 0.066$	0.985	0.943	1.02
110 ± 7		$5.24 \pm 0.03 \pm 0.13$	$-0.307 \pm 0.011 \pm 0.018$	0.982	0.933	1.02
130 ± 7		$5.95 \pm 0.03 \pm 0.09$	$-0.270 \pm 0.009 \pm 0.022$	0.972	0.896	1.02
148 ± 7		$7.32 \pm 0.03 \pm 0.31$	$-0.208 \pm 0.007 \pm 0.009$	0.941	0.779	1.02
166 ± 7		$7.57 \pm 0.03 \pm 0.10$	$-0.084 \pm 0.009 \pm 0.005$	0.590	0.101	1.01
16 ± 8		$5.56 \pm 0.02 \pm 0.18$	$-0.076 \pm 0.011 \pm 0.024$	0.536	0.072	1.01
32 ± 8		$5.26 \pm 0.02 \pm 0.18$	$-0.167 \pm 0.006 \pm 0.004$	0.905	0.679	1.02
51 ± 8		$4.49 \pm 0.02 \pm 0.03$	$-0.259 \pm 0.007 \pm 0.005$	0.959	0.843	1.02
71 ± 8		$3.74 \pm 0.02 \pm 0.16$	$-0.279 \pm 0.010 \pm 0.023$	0.972	0.890	1.03
90 ± 8	180–200	$3.38 \pm 0.02 \pm 0.14$	$-0.339 \pm 0.008 \pm 0.024$	0.974	0.902	1.03
109 ± 8		$3.69 \pm 0.02 \pm 0.12$	$-0.310 \pm 0.008 \pm 0.029$	0.971	0.886	1.03
129 ± 8		$4.08 \pm 0.02 \pm 0.19$	$-0.215 \pm 0.007 \pm 0.006$	0.956	0.833	1.03
148 ± 9		$5.09 \pm 0.02 \pm 0.12$	$-0.150 \pm 0.006 \pm 0.007$	0.904	0.661	1.02
163 ± 8		$5.76 \pm 0.02 \pm 0.02$	$-0.096 \pm 0.009 \pm 0.006$	0.561	0.043	1.01
22 ± 14		$2.34 \pm 0.02 \pm 0.06$	$-0.114 \pm 0.031 \pm 0.042$	0.366	-0.129	1.02
37 ± 12		$2.04 \pm 0.02 \pm 0.05$	$-0.143 \pm 0.017 \pm 0.010$	0.725	0.303	1.03
54 ± 12		$1.77 \pm 0.02 \pm 0.02$	$-0.194 \pm 0.015 \pm 0.011$	0.833	0.533	1.04
72 ± 11		$1.57 \pm 0.01 \pm 0.09$	$-0.253 \pm 0.016 \pm 0.025$	0.881	0.646	1.05
91 ± 11	200–220	$1.48 \pm 0.01 \pm 0.08$	$-0.255 \pm 0.016 \pm 0.038$	0.896	0.677	1.05
109 ± 11		$1.54 \pm 0.01 \pm 0.12$	$-0.233 \pm 0.015 \pm 0.028$	0.894	0.664	1.05
127 ± 13		$1.67 \pm 0.01 \pm 0.13$	$-0.168 \pm 0.015 \pm 0.006$	0.848	0.546	1.04
143 ± 13		$1.89 \pm 0.02 \pm 0.10$	$-0.164 \pm 0.016 \pm 0.011$	0.730	0.305	1.03
157 ± 15		$2.04 \pm 0.02 \pm 0.22$	$-0.120 \pm 0.032 \pm 0.066$	0.349	-0.130	1.02

To quantify the changes caused by the φ_q variation, we define a correction factor d_t using Eq. (5),

$$d_t \equiv \sigma_0(\langle \cos 2\varphi_q \rangle)/\sigma_0(\cos 2\varphi_q = 1). \tag{7}$$

The d_t values given in our Table I were obtained for our kinematic conditions by interpolating the coefficients quoted in Table IV of the IUCF work [2]. It must be noted that the value of H_3^{00} appearing in Eq. (5) could not be determined in the IUCF work and the value is assumed to be zero in the analysis. The calculations show that the cross section increases as φ_q moves away from 0° and hence that the analyzing power decreases.

The spin-averaged cross sections and analyzing powers found by integrating over the polar angles θ_q are shown as functions of the relative momentum p in Table II. The mean values and uncertainties in the determination of p have been estimated in the same way as for the pion polar angle θ_q in Table I. The spin-averaged cross sections and analyzing powers have been obtained at average values of $\cos 2\varphi_q$, which depend upon $\cos \theta_q$, and they must be subjected to a correction factor d_t, similar to that given in Table I, to extrapolate the results to $\cos 2\varphi_q = 1$.

VI. DISCUSSION

A. Angular dependence

The variation of the spin-averaged cross section with pion angle is shown in Fig. 8 for the three momentum ranges. Since, for this purpose, the two initial protons are identical, the data are presented as functions of $\cos^2 \theta_q$. The variation seems to be linear, as expected on the basis of Eq. (5), and the data were therefore fit with the form

$$\sigma_0 = \alpha(1 + c \cos^2 \theta_q). \tag{8}$$

The resulting parameters with and without the d_t factor are given in Table III. In all cases the χ^2/d.o.f. were close to unity.

TABLE II. The $pp \to pp\pi^0$ spin-averaged cross section, $d\sigma/d\varphi_q d\Omega_p dp$, after integration over θ_q, presented in different bins of the relative momentum p. The corresponding integrated values of the analyzing power A_y are also given. The first and second error bars denote the statistical and systematic uncertainties, respectively, whereas that on the relative momentum p is the standard deviation that includes the effects of the binning. The observables were measured over a range of φ_q and, to get estimates of the values at $\cos 2\varphi_q = 1$, the cross section should be divided by the correction factor d_t and the analyzing power multiplied by the same factor, as discussed for Table I.

p (MeV/c)	$d\sigma/d\varphi_q d\Omega_p dp$ [nb/(rad sr MeV c^{-1})]	A_y	d_t
155 ± 4	$12.33 \pm 0.04 \pm 1.37$	$-0.278 \pm 0.005 \pm 0.014$	1.02
165 ± 4	$12.39 \pm 0.03 \pm 0.28$	$-0.283 \pm 0.004 \pm 0.018$	1.02
175 ± 4	$10.88 \pm 0.03 \pm 0.24$	$-0.266 \pm 0.004 \pm 0.011$	1.02
185 ± 4	$9.52 \pm 0.02 \pm 0.13$	$-0.251 \pm 0.004 \pm 0.005$	1.02
195 ± 4	$7.42 \pm 0.02 \pm 0.19$	$-0.223 \pm 0.004 \pm 0.010$	1.03
205 ± 4	$4.76 \pm 0.02 \pm 0.15$	$-0.203 \pm 0.006 \pm 0.011$	1.04
214 ± 4	$2.12 \pm 0.01 \pm 0.13$	$-0.136 \pm 0.010 \pm 0.040$	1.03

The results, with and without the d_t modification, are both consistent with c being constant.

The angular distribution of the pion has been investigated by several experimental groups in the 400-MeV region, though with somewhat conflicting conclusions regarding the slope parameter c. Thus $c = 0.28 \pm 0.20$ was found at IUCF [2], 0.19 ± 0.01 at TSL (PROMICE-WASA) [4], -0.35 ± 0.03 at TSL (WASA) [5], and -0.19 ± 0.02 at COSY-TOF [7]. In the last of these experiments, a dependence of the parameter upon the relative momentum could be established, with c changing from negative to positive as p increases. However, even the TOF result of 0.09 ± 0.01 obtained for $p > 160$ MeV/c is significantly smaller than ours for a similar momentum range. This difference can be explained in terms of the different geometries of the two experiments.

Whereas at COSY-TOF the full phase space was explored, our data were taken in essentially coplanar conditions (i.e., $\varphi_p = \varphi_q = 0^\circ$), and with the proton polar angle of $\theta_p = 90^\circ$. Using Eq. (5) with the coefficients taken from Table IV of the IUCF work [2], one can derive a relation between the slope parameter (c) for full acceptance and the value ($c^\star$) to be found with our limited coverage. Since H_5^{00} is negative [2], $c^\star$ is always larger than c and for $p > 160$ MeV/c one expects that $c^\star \approx 0.3 + 3.0\,c$. Using this relation with the COSY-TOF value of c, one can predict a value of $c^\star = 0.57 \pm 0.03$, which is consistent with our results.

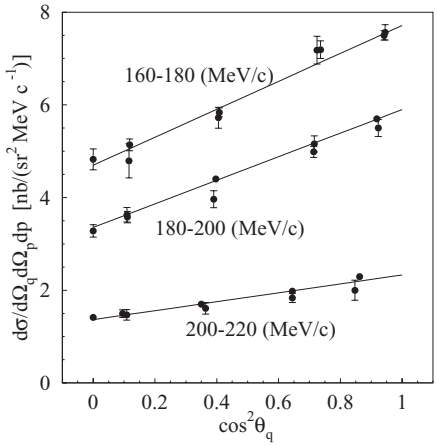

FIG. 8. The angular dependence of the spin-averaged $pp \to pp\pi^0$ cross section for the three regions of relative momentum indicated. The error bars include the statistical and systematic uncertainties. The solid lines show the results of fitting the data with the linear form of Eq. (8), with the resulting parameters being given in Table III.

The sign of the slope parameter c is positive for high p, reflecting the importance there of the Pp contribution. However, both the TSL [4] and COSY-TOF [7] data show that c is negative for $p < 53$ MeV/c, probably owing to an $SsSd$ interference that falls very fast with increasing p.

Figure 9 presents the dependence of A_y on the pion polar angle for the three relative-momentum regions. The solid line shows the fits resulting from using the general angular dependence of Eq. (6),

$$\sigma_0 A_y = a \sin\theta_q + b \sin 2\theta_q, \tag{9}$$

where the values of the free parameters a and b are listed in Table III. In the fitting, the uncertainty in the angular determination has been included in the χ^2 minimization.

It is seen from Table III that b is consistent with zero for all three momentum bins. Since the parameters a and b correspond, respectively, to the $PsPp$ and ($SsSd$, $PpPp$) contributions in Eq. (6), this shows clearly that, for the large values of p investigated in our experiment, the $PsPp$ interference terms dominate.

If the values of all the coefficients given in Table IV of Ref. [2] are inserted into Eqs. (5) and (6), these predict the angular dependence shown in Fig. 9. The upper and lower dotted lines are obtained by using the numbers corresponding to 375 and 400 MeV, respectively. It must be noted that the IUCF parameters were obtained from averages of A_y over the

TABLE III. Parameters extracted by fitting the angular dependence of $\sigma_0(\theta_q)$ and $\sigma_0 A_y(\theta_q)$ with Eqs. (8) and (9), respectively. The values in brackets show the results obtained when the correction factor d_t is included in the fitting process.

p (MeV/c)	α [nb/(sr^2 MeV c^{-1})]	c	a [nb/(sr^2 MeVc^{-1})]	b/a
160–180	$4.82 \pm 0.10 (4.70 \pm 0.10)$	$0.62 \pm 0.04 (0.64 \pm 0.05)$	-2.00 ± 0.12	0.05 ± 0.06
180–200	$3.47 \pm 0.05 (3.35 \pm 0.06)$	$0.72 \pm 0.03 (0.76 \pm 0.04)$	-1.23 ± 0.06	0.04 ± 0.07
200–220	$1.44 \pm 0.04 (1.37 \pm 0.04)$	$0.64 \pm 0.08 (0.71 \pm 0.09)$	-0.40 ± 0.03	0.06 ± 0.11

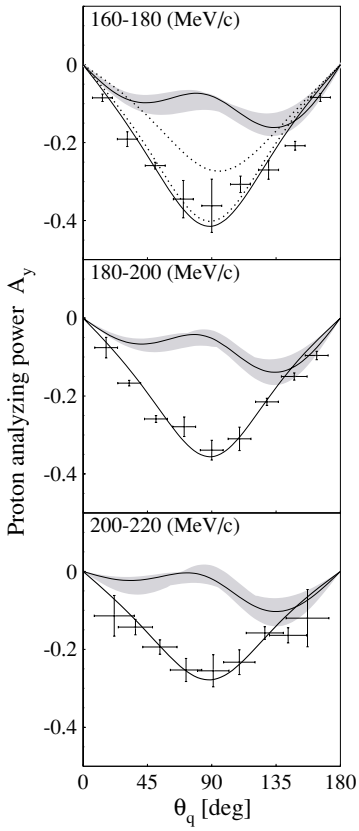

FIG. 9. The dependence of the $\vec{p}p \to pp\pi^0$ analyzing power on the pion polar production angle θ_q for the three regions of relative momenta of the final protons. The error bars include the statistical and systematic uncertainties. The solid curves are fits of Eqs. (8) and (9) to these and the data of Fig. 8, with the resulting parameters being given in Table III. The upper and lower dotted curves in the lowest momentum region have been calculated from Eqs. (5) and (6) by using the coefficients given in Ref. [2] at 375 and 400 MeV, respectively. The curves bordered by shaded areas are the theoretical results from the Osaka group, with the shading indicating the expected uncertainties in the calculation [20].

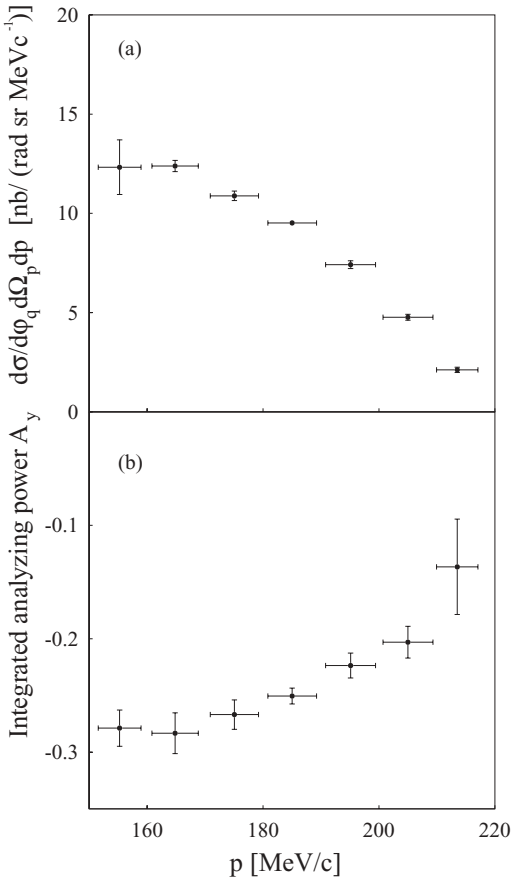

FIG. 10. (a) Spin-averaged cross section as a function of the relative momentum of the final protons. (b) The relative momentum dependence of the integrated analyzing power. The error bars include the statistical and systematic uncertainties.

full range of allowed proton-proton relative momenta [2]. The close agreement found in the 160–180 MeV/c bin when using the 400-MeV coefficients is due, in part, to the cross section being maximal in this region.

In contrast, the model calculations of the Osaka group [20], shown in Fig. 9, demonstrate a much more asymmetrical behavior than the experimental data and greatly underestimate the magnitude of the analyzing power. The predictions for the Pp or Ps transitions are therefore much smaller than those found experimentally. More theoretical studies are needed to elucidate the origin of this disagreement.

B. Momentum dependence

Figures 10(a) and 10(b) show, respectively, the spin-averaged cross section and analyzing power integrated over θ_q as functions of the relative momentum of the final protons. The error bars include both systematic and statistical uncertainties. On kinematic grounds, A_y must tend to zero as p approaches the highest allowed values because the pion momentum vanishes in this limit. As previously remarked, the cross section seems to be maximal at our lowest values of p, as does the magnitude of the analyzing power.

VII. PHENOMENOLOGICAL ANALYSIS

It was already stressed that the combination $\sigma_0 A_y$ is not sensitive to the $\cos 2\varphi_q$ term in Eq. (5) and so does not suffer from the resultant d_t ambiguity. Since the integral of the $\sin 2\theta_q$ term in Eq. (9) over the pion angle vanishes, the dependence of the integrated $\sigma_0 A_y(p)$ can be expressed in terms of the interference between the two types of P-state amplitudes multiplied by the three-body phase-space factor $\rho(p)$:

$$\sigma_0 A_y(p) = PsPp\ \rho(p). \tag{10}$$

This $PsPp$ corresponds to a linear combination of the coefficients $G^{y0}_{1,2,4}$ in Eq. (6). According to Ref. [2], G^{y0}_1, which does not contain any θ_p dependence, contributes about 95% of the total magnitude of A_y so that to a good approximation the $G^{y0}_{2,4}$ may be neglected. In this case, $PsPp$ results from s-p interferences with the same P states of the final protons. It can

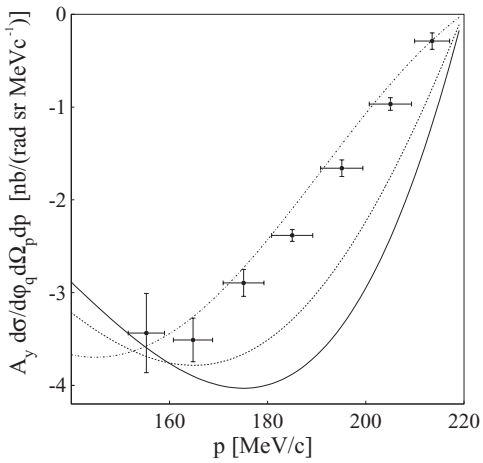

FIG. 11. The relative momentum dependence of the angle-integrated $A_y\sigma_0(p)$. The error bars include the statistical and systematic uncertainties. The lines show the variation predicted for the $^3P_2$ state when using Eq. (13) with different values of the interaction range. The solid line shows the calculation with $R = 1$ fm, whereas the dashed line and dot-dashed line show the calculations with $R = 2$ fm and $R = 3$ fm, respectively.

therefore be expressed as

$$PsPp = C_0\, f_{^3P_0 s}\, f_{^3P_0 p} + C_2\, f_{^3P_2 s}\, f_{^3P_2 p}, \tag{11}$$

where $C_{0,2}$ are parameters and $f_{^3P_{0,2}s}$ and $f_{^3P_{0,2}p}$ represent the pion s- and p-wave amplitudes, respectively.

A partial-wave amplitude for pion production may be approximated in terms of the overlap integral involving the pion-production operators $\hat{\Pi}(r)$ and the radial wave function of initial and final protons [$u_i(r)$ and $u_f^p(r)$] and the pion plane wave $j_l(\frac{1}{2}qr)$:

$$f_{fl} = \int u_f^p(r)\, j_l\left(\frac{1}{2}qr\right)\, \hat{\Pi}(r)\, u_i(r)\, r^2\, dr, \tag{12}$$

where r is the proton-proton separation distance, and l and q are the pion angular momentum and momentum, respectively. Analytic forms for the Ss-wave pion-production amplitude may be found in Ref. [10].

If the pion-production operator is taken to be momentum-independent, any strong momentum dependence of the partial-wave amplitude must be ascribed to the variation of the radial wave function of the final protons and pion with p and q. To investigate this further, we approximate Eq. (12) by evaluating the product of the wave functions at a *fixed* distance $r = R$, in which case

$$f_{fl} \propto u_f^p(R)\, j_l\left(\tfrac{1}{2}qR\right). \tag{13}$$

The $^3P_{0,2}$ radial wave functions have been derived from the Paris potential with the Coulomb interaction [27]. Since the experimental data cannot distinguish between the contributions from the $^3P_0$ and $^3P_2$ states, the calculations have been carried out by taking them into account one at a time. However, there is very little difference between the two sets of results and only those for the $^3P_2$ states are shown in Fig. 11. The overall normalization factor $C_{0,2}$ has been fixed on the basis of Eq. (6) to satisfy $\int \sigma_0 A_y(p)dp = \sigma_{\rm tot}\,(G_1^{y0} - G_2^{y0} + G_4^{y0})/16\pi$, where the value $\sigma_{\rm tot} = 65\ \mu$b has been obtained by interpolation of the IUCF data [2].

The $\sigma_0 A_y$ data are only sensitive to a value of the distance $R = R_{Ps} = R_{Pp}$. As demonstrated in Fig. 11, the curves obtained from Eq. (13) by using radii $R = 1$, $R = 2$, and $R = 3$ fm show significantly different dependencies on the relative momentum. The $R = 1$ fm line fails to reproduce the data but, as R is increased, the minimum in the curve moves toward lower momenta and the data are better described. Within the framework of this simplistic analysis, the data seem to require a pion-production operator with a fairly long range component. It was noted for the TSL measurements of the differential cross section $d\sigma/dp$ [4] that the momentum dependence could be described by taking the exchanged particle in Eq. (12) to have the mass of the pion but that such a description was no longer possible when the ρ-meson mass was used.

VIII. SUMMARY

We have measured the angular and momentum dependence of the cross section and analyzing power of the $\vec{p}p \to pp\pi^0$ reaction at an incident energy of 390 MeV. Recoil protons stopped in a scintillation counter have been identified by the ΔE-E technique. Though the counters in the horizontal plane covered angles between 15° and 35° to the left and right of the beam, the vertical acceptance was quite small and this feature is crucial in any theoretical description of the data. Only high relative momentum $p > 160$ MeV/c were registered and, under these conditions, final P-state proton pairs play an important role.

Although the dependence of the cross section on the pion angle shows a larger anisotropy than in the case of data obtained with almost full acceptance [2,4,7], this is in large part the result of our coplanar geometry. After we take this into account by using the IUCF parameters [2], our results do not contradict those recently published by COSY-TOF [7].

The shape of $\sigma_0 A_y(\theta_q)$ follows quite closely a $\sin\theta_q$ form, which is consistent with this observable being dominated by $PpPs$ interference. The contribution from the $SsSd$ term is negligible at the high relative momentum studied in this experiment. However, the behavior of A_y at small p could be a useful probe to investigate the role of the $SsSd$ contribution [28].

The momentum dependence of the analyzing power at large p is also consistent with the $PpPs$ interference interpretation. The variation can be explained within a very simple model by taking the pion-production operator to have a rather long range.

Our results, taken in conjunction with the IUCF double-polarized data [2] and other published results on the unpolarized cross sections, may provide the extra information necessary for the understanding of the production mechanisms for P-state protons. However, to succeed in this, a much more sophisticated theoretical model is required to replace the rather qualitative approach used here to describe the data.

ACKNOWLEDGMENTS

The authors are grateful to the cyclotron staff for their support throughout this experiment. We acknowledge the help of K. Sagara with the liquid hydrogen target system. Comments from Professor A. Johansson have been particularly valuable. This work was performed at RCNP under the program E140.

[1] H. O. Meyer *et al*., Phys. Rev. Lett. **65**, 2846 (1990); Nucl. Phys. **A539**, 633 (1992).
[2] H. O. Meyer *et al*., Phys. Rev. C **63**, 064002 (2001).
[3] A. Bondar *et al*., Phys. Lett. B **356**, 8 (1995).
[4] R. Bilger *et al*., Nucl. Phys. **A693**, 633 (2001).
[5] P. Thörngren Engblom *et al*., Phys. Rev. C **76**, 011602(R) (2007).
[6] S. Abd El-Samad *et al*., Eur. Phys. J. A **17**, 595 (2003).
[7] S. Abd El-Samad *et al*., Eur. Phys. J. A **30**, 443 (2006).
[8] G. A. Miller and P. U. Sauer, Phys. Rev. C **44**, R1725 (1991).
[9] T.-S. H. Lee and D. O. Riska, Phys. Rev. Lett. **70**, 2237 (1993).
[10] C. J. Horowitz, H. O. Meyer, and D. K. Griegel, Phys. Rev. C **49**, 1337 (1994).
[11] E. Hernandez and E. Oset, Phys. Lett. **B350**, 158 (1995).
[12] C. Hanhart, J. Haidenbauer, O. Krehl, and J. Speth, Phys. Lett. **B444**, 25 (1998).
[13] B.-Y. Park, F. Myhrer, J. R. Morones, T. Meissner, and K. Kubodera, Phys. Rev. C **53**, 1519 (1996).
[14] T. D. Cohen, J. L. Friar, G. A. Miller, and U. vanKolck, Phys. Rev. C **53**, 2661 (1996).
[15] U. vanKolck, G. A. Miller, and D. O. Riska, Phys. Lett. **B388**, 679 (1996).
[16] T. Sato, T.-S. H. Lee, F. Myhrer, and K. Kubodera, Phys. Rev. C **56**, 1246 (1997).
[17] C. Hanhart, U. vanKolck, and G. A. Miller, Phys. Rev. Lett. **85**, 2905 (2000).
[18] C. Hanhart and N. Kaiser, Phys. Rev. C **66**, 054005 (2002).
[19] C. Hanhart, J. Haidenbauer, O. Krehl, and J. Speth, Phys. Lett. **B444**, 25 (1998); Phys. Rev. C **61**, 064008 (2000).
[20] K. Tamura, Y. Maeda, and N. Matsuoka, Nucl. Phys. **A663-664**, 457c (2000); Y. Maeda, N. Matsuoka, and K. Tamura, Nucl. Phys. **A684**, 392c (2001).
[21] P. N. Deepak, J. Haidenbauer, and C. Hanhart, Phys. Rev. C **72**, 024004 (2005).
[22] K. Hatanaka *et al*., Nucl. Instrum. Methods Phys. Res. A **384**, 575 (1997).
[23] Y. Sugaya and M. Nomachi, Nucl. Instrum. Methods Phys. Res. A **437**, 68 (1999).
[24] R. A. Arndt, I. I. Strakovsky, and R. L. Workman, Phys. Rev. C **50**, 2731 (1994).
[25] K. Sagara *et al*., RCNP Annual Report, 1995, p. 158.
[26] F. G. de Bilio, GEANT3 manual, CERN Program Library Long Writeup W5013, October 1994.
[27] M. Lacombe *et al*., Phys. Rev. C **21**, 861 (1980).
[28] A. Kulikov *et al*. COSY Proposal 158, 2006, http://www.fz-juelich.de/ikp/anke/en/proposals.shtml.